Perturbation Pressure at the Base of Cumulus Clouds in Low Shear

MARGARET A. LEMONE, LESLEY F. TARLETON* AND GARY M. BARNES

*The National Center for Atmospheric Research,** Boulder, Colorado*

(Manuscript received 6 November 1987, in final form 21 March 1988)

ABSTRACT

We examine the pressure fields around the cloud-base updraft of three cumulus clouds observed in environments with low vertical shear of the horizontal wind near cloud base. These fields are compared to the corresponding pressure fields beneath convective clouds embedded in moderate to large shear. All of the pressure fields are derived from aircraft measurements taken during the 1981 Cooperative Convective Experiment, CCOPE.

The pressure fields associated with these low-shear clouds are weaker than those for the clouds in higher shear. Furthermore, the low-shear fields are not consistently dominated by the dynamic pressure created by the interaction of the cloud-base updraft with the vertical shear of the horizontal wind. The weaker dynamic pressure is due to the smaller size and intensity of the cloud-base updraft as well as the smaller vertical shear of the horizontal wind. The reduction of the dynamic pressure allows buoyancy effects on the pressure field to become more apparent.

1. Introduction

LeMone et al. (1988) showed that the perturbation pressure field around the cloud-base updraft of deep convective clouds in moderate to strong shear is a high–low couplet bracketing the updraft, with the low pressure on the updraft's downshear side. The pressure perturbation was found to be due mainly to the interaction of the updraft with the vertical shear of the horizontal wind. The magnitude of the pressure perturbation was proportional to the updraft speed and diameter, and the vertical shear of the horizontal wind at cloud base, measured in the direction of the maximum pressure change. The studied updrafts varied in diameter from 5 to 20 km, and in intensity from 5 to 9 m s^{-1}. The vertical shear of the environmental horizontal wind at cloud base ranged from 3.5 to 9.4 $\times 10^{-3}$ s^{-1}.

Surprised at the consistency of the results over such a large range of parameters, we have selected three clouds in low shear as "controls", to see how the pressure field differs. We calculate the pressure using the same technique as LeMone et al. (1988), which is described in detail in LeMone and Tarleton (1986).

We show here that the pressure fields in the low-shear clouds are extremely weak and often cannot be separated from the noise. Only one of the three clouds shows a hint of the high–low pressure couplet bracketing the updraft, as found in the higher-shear clouds. In the other two cases, lower pressures strongly overlap with cloud overhead, suggesting buoyancy to be the main pressure-perturbation source. We attribute the lesser importance of shear-updraft interaction to the size of the updrafts as well as the reduced shear: the low-shear clouds have updraft diameters and speeds less than or equal to those for the smallest clouds analyzed in LeMone et al. (1988). In fact, the size and magnitude of the updrafts and pressure fields for these small clouds fall between those for the deep convective clouds studied by LeMone et al. and those associated with fair weather boundary-layer eddies. Thus we speculate that the causes of the small-cloud pressure fields are also intermediate between those for large clouds and those for boundary-layer eddies.

2. Sampling and data-analysis procedure

a. Measurements

Measurements from the NCAR Queen Air 306 during the Cooperative Convective Precipitation Experiment (CCOPE) provide the perturbation pressure and vertical-velocity fields at cloud base. The flight patterns are across and along the major axis of the cloud and centered upon the updraft, as described by LeMone et al. (1988). Cloud edges are from aircraft time-lapse (one frame each 4 sec) films taken out the front of the aircraft (Fankhauser et al. 1983).

Rawinsondes are used to obtain the environmental wind and thermodynamic profiles. Environmental

* Present affiliation, Department of Geography, University of Oklahoma, Norman, Oklahoma.

** The National Center for Atmospheric Research is sponsored by the National Science Foundation.

Corresponding author address: Dr. Margaret A. LeMone, NCAR, P.O. Box 3000, Boulder, CO 80307.

soundings are chosen on the basis of location relative to the cloud, and agreement of the lifted parcel thermodynamic properties with those properties measured beneath the cloud by the aircraft. The aircraft-measured cloud-base mixing ratio is used for parcel trajectories, rather than the average boundary-layer mixing ratio from the rawinsonde. The wind profiles are low-pass filtered using the "macro-pass" filter of Madden et al. (1971). The filter response falls off from unity at a vertical distance of about 4 km to zero at 1.7 km. Thus the shear through cloud base is representative of the upper boundary layer and lower cloud layer.

b. Calculations of the perturbation pressure field

The perturbation pressure is found from the "D-value", via:

$$p' = \rho g D \tag{1}$$

where D is the actual altitude of the aircraft, minus its pressure altitude. The actual altitude is found from integrating the aircraft's vertical acceleration, while the pressure altitude is found from the aircraft-measured pressure and a vertical sounding representative of the environment.

Because errors of unknown origin occur in turns, the actual altitude is calculated separately for each straight and level flight leg. In the integration, the initial altitude is assumed equal to the pressure altitude. The data are then linearly detrended, so that the final altitudes also match. The D value is then computed. Because the accelerometers have a roughly constant bias, the resulting D values are superimposed on a quadratic. Thus the D values are quadratically detrended, under the constraint that the D value is zero at both ends of each flight leg. Based upon in-flight calibration maneuvers, the estimated perturbation-pressure error is of the order of 20 Pa. Since aircraft maneuvers are less extreme in smaller clouds, the achievable accuracy is probably better for the clouds presented here. Further details of the calculation and error estimation appear in LeMone and Tarleton (1986).

c. Analysis of perturbation pressure fields

Of the three clouds analyzed, two occurred on 12 July and one on 18 July 1981. For two of the clouds—cloud 2 of 12 July and the cloud of 18 July—the smoothed vertical velocity and pressure perturbation fields are plotted relative to the main updraft. Motions of scales less than 1 to 2 km are ignored for the 12 July clouds, and less than 1 km for the 18 July cloud. Analyses are done on sequential legs which show a similar updraft signal. Flight-leg statistics in Fankhauser et al. (1983) reveal that the internally consistent analyses correspond with periods for which the maximum vertical velocities are steady to within 2 m s^{-1}.

Cloud 1 of 12 July is analyzed in earth-relative coordinates. We do this because the flight pattern, the association of the cloud with a line, and the clouds' slow movement all made the main updraft difficult to track. Fortunately, the slow movement also minimizes the problems with using an earth-relative coordinate system: the only adverse result is a slight stretching of features along the direction of motion (probably toward the northwest). Three legs along the cloud line were flown within the first 13 minutes. During this time, the system was steady to within the previously-mentioned criteria. The cross-line runs, flown during the next eight minutes, revealed much weaker vertical velocities. This is mainly due to the fact that the two cross-axis runs skirt the main updraft, but time changes are probably involved as well. Unfortunately, these legs are the only source of information on the structure across the entire cloud line.

The analysis time and the total sampling time for each cloud are listed in Table 1. From Table 1, all analyses involve greater than half the sampling time, a rough measure of cloud lifetime. For comparison, the analysis times for the higher-shear clouds presented in LeMone et al. (1988) varied from 30% of the cloud

TABLE 1. Summary of cases presented.

Date	Analysis times MDT (total time spent sampling cloud)	Altitude[a] of observations (m MSL)	Pressure (mb)	T_v (°K)	Shear through cloud base[b] dU/dz ($\times 10^{-3}$ s^{-1})	Shear through cloud base[b] dV/dz ($\times 10^{-3}$ s^{-1})
12 July–Cloud 1	1406:00–1427:20[c] (1406:00–1444:38)	2140	780	290	1.8	0.4
12 July–Cloud 2	1453:46–1507:51 (1453:46–1514:45)	2270	770	290	1.8	0.4
18 July	1518:51–1526:14 (1512:30–1526:14)	2680	730	284	1.2	−0.7

[a] Surface is at about 900 m.
[b] U positive east, V positive north.
[c] First three legs 1406–1419:14.

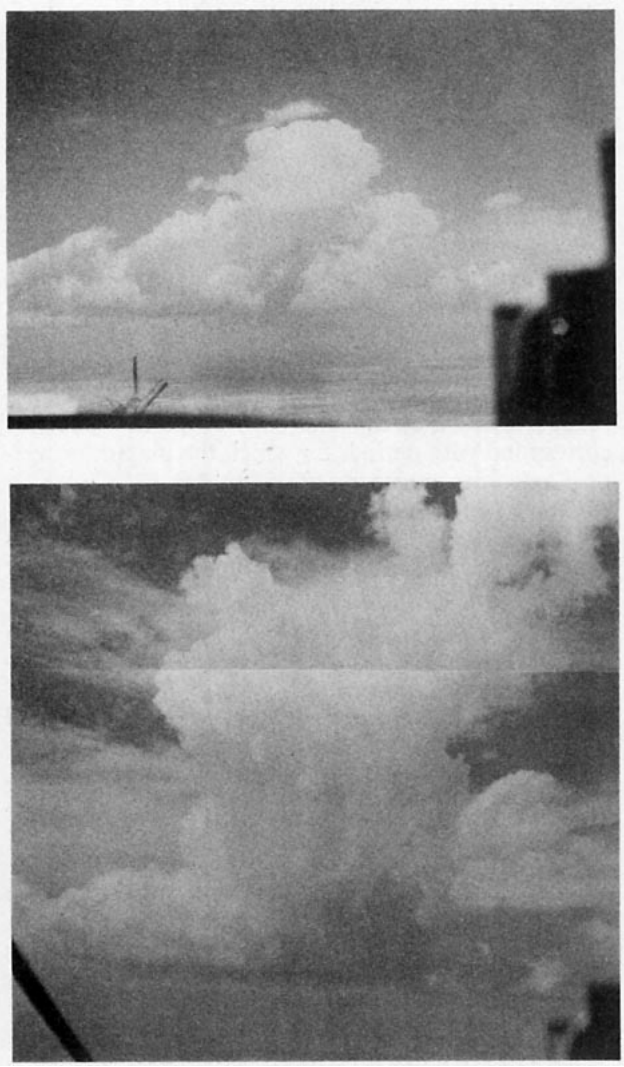

FIG. 1. Clouds of 12 July. (a) Cloud 1 at 1404 MDT, taken from Queen Air 306D looking NE at 1950 m, about 300 m below cloud base. (b) Cloud 2 at 1502:30 MDT looking SW at 2270 m, just below cloud base. Photos by J. C. Fankhauser, NCAR.

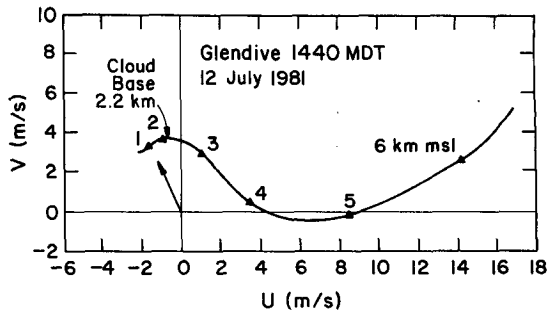

FIG. 2. Hodograph for 12 July 1981 clouds. Arrow indicates estimated motion of cloud 2. Cloud 1 motion could not be determined accurately (see text). The clouds are about 30 km south of Glendive.

lifetime to less than 10%. Thus, the clouds discussed below probably evolved faster during analysis times than the higher-shear clouds. For this reason we filtered out the smaller, more transient features. This is probably why the perturbation pressures at overlapping or nearly-overlapping points in the flight pattern usually agree to better than 5 Pa. Nevertheless, we will minimize stationarity problems by discussing only the broadest features of the pressure and vertical velocity patterns presented below.

3. Results

For the three clouds studied, Table 1 lists the flight and analysis times, the mean height of the aircraft, and the static pressure and virtual temperature sensed by the aircraft, which was flying 50 to 100 m below cloud base, and the vertical shear of the horizontal wind through cloud base. The days were selected for analysis because of the low vertical shear of the horizontal wind at cloud base; the clouds were selected on the basis of the number of aircraft passes. We describe the clouds chronologically.

(i) 12 July: Figure 1 shows the two clouds analyzed for this day. Cloud 1 (Fig. 1a) is part of a line of clouds, while cloud 2 (Fig. 1b) is isolated. The environmental hodograph and thermodynamic profiles are shown in Figs. 2 and 3. The total shear at flight level (1.8×10^{-3} s^{-1} from Table 1), is smaller than that for the clouds

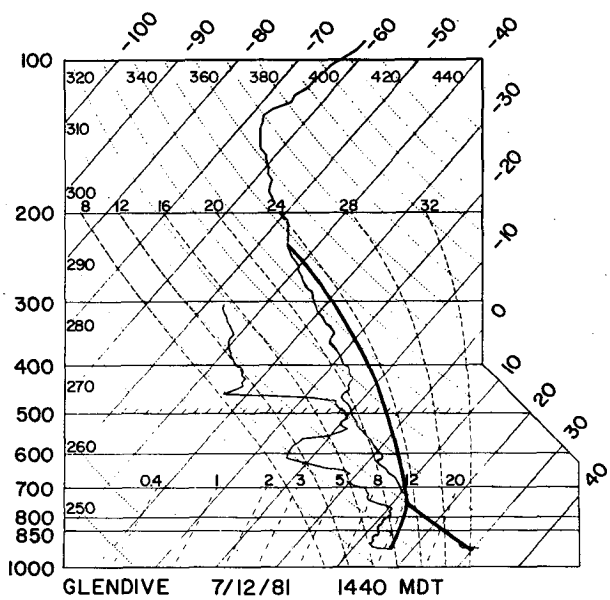

FIG. 3. Temperature and mixing ratio profiles corresponding to hodograph in Fig. 2, on a skew T–log$p$ diagram. Dotted lines are dry adiabats, closely dashed lines are moist adiabats, diagonal lines slanting to the right are temperature, and loosely dashed lines are mixing ratio. Heavy lines show the path of undilute air parcel with thermodynamic properties consistent with those measured by the aircraft at cloud base.

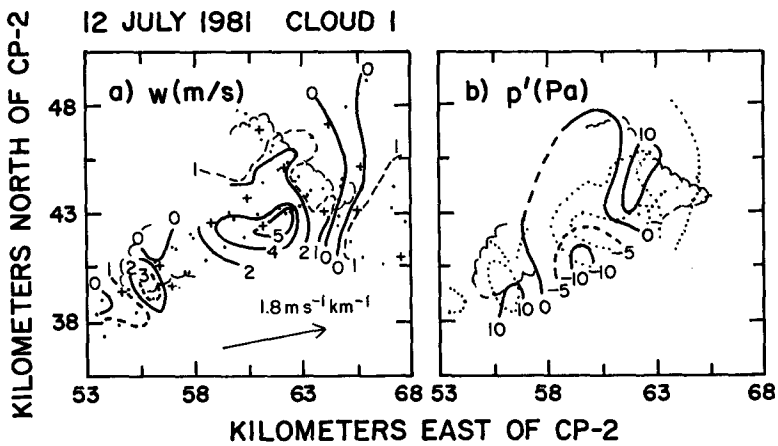

FIG. 4. For 12 July, just below base of cloud 1: (a) vertical velocity field, and (b) perturbation pressure fields with vertical velocity (dotted) superimposed. Cloud base is outlined in scallops. For times and pattern altitude, see Table 1. The fields are plotted in earth-relative coordinates; flight tracks [dots and crosses] are superimposed on (a). The vector indicates the vertical shear of the horizontal wind from Fig. 2, evaluated at cloud base.

in LeMone et al. (1988), which varies from 3.5 to 9.4 $\times 10^{-3}$ s^{-1}.

Cloud 1 (Fig. 1a) towered over its neighbors, with turrets reaching 5.7 km MSL (Alan Blyth via Jørgen Jensen, personal communication 1987). The vertical velocity and pressure field at its base appear in Figs. 4a and 4b. The figure is plotted in earth-relative coordinates, since cloud motion could not be determined accurately but was near zero. The scallops outline the envelope of the data beneath cloud base. Since there were several clouds in the line, the scallops probably outline more than one cloud.

Note that more than one updraft feeds the clouds. The pressure fields are weak and mostly below the 20-Pa error threshold quoted in LeMone and Tarleton (1986). As mentioned previously, both fields probably evolve during sampling. Thus the fields should be interpreted with caution. Nevertheless, the consistency of the data from leg to leg and the smaller potential errors associated with these weaker clouds give us confidence in the qualitative results. The cloud, updraft, and low pressure show strong overlap, with the pressure minimum *upshear* of the main updraft, rather than downshear as observed in LeMone et al. (1988).

Figures 5a and 5b show the vertical velocity and perturbation pressure fields for the isolated cloud 2. This cloud moved toward the NNW at about 2 m s^{-1}. There are several updraft maxima, the strongest of which lies beneath the cloud base. The pressure field is weak and noisy, but with a consistent high-low couplet bracketing the main updraft, with the lowest pressure on the downshear side, as in the higher-shear LeMone et al. (1988) clouds.

(ii) 18 July: The environmental hodograph and thermodynamic profiles for the 18 July cloud appear in Figs. 6 and 7. Based on the aircraft film, the cloud top reaches around 5 to 5.5 km MSL. In this case, the cloud moves from 286 deg at 5.5 m s^{-1}, a velocity very close to the cloud-base wind. From Table 1, the cloud-base shear is even smaller than for 12 July.

Figure 8 shows the vertical velocity and pressure-perturbation fields for this cloud. The lower pressures are beneath the cloud base, with the lowest values on the upshear side. Small areas of high pressure lie on both sides of the cloud.

4. Discussion

The pressure fields of Figs. 4, 5, and 8 are very weak. Only cloud 2 in Fig. 5 behaves as if shear–updraft interaction is an important source of the pressure field, with the telltale high–low couplet around the main updraft. The other two clouds share a tendency for lower pressure beneath cloud base.

Why do the low-shear clouds behave differently from the higher-shear clouds described in LeMone et al. (1988)? To answer this, we refer to the shallow-layer anelastic approximation of the Poisson equation, written for an adiabatic environment (Rotunno and Klemp 1982; R. Rotunno, personal communication 1987):

$$-\nabla^2\left(\frac{p'}{\rho_e}\right) = \left(\frac{\partial u}{\partial x}\right)^2 + \left(\frac{\partial v}{\partial y}\right)^2 + \left(\frac{\partial w}{\partial z}\right)^2 + 2\frac{\partial u}{\partial y}\frac{\partial v}{\partial x} + 2\frac{\partial u}{\partial z}\frac{\partial w}{\partial x} + 2\frac{\partial v}{\partial z}\frac{\partial w}{\partial y} - \frac{\partial B}{\partial z} \quad (2)$$

where p' is the pressure perturbation, ρ_e the density of the environmental air, B the buoyancy, and u, v and w are the components of the wind, here in a right-hand coordinate system with u positive east.

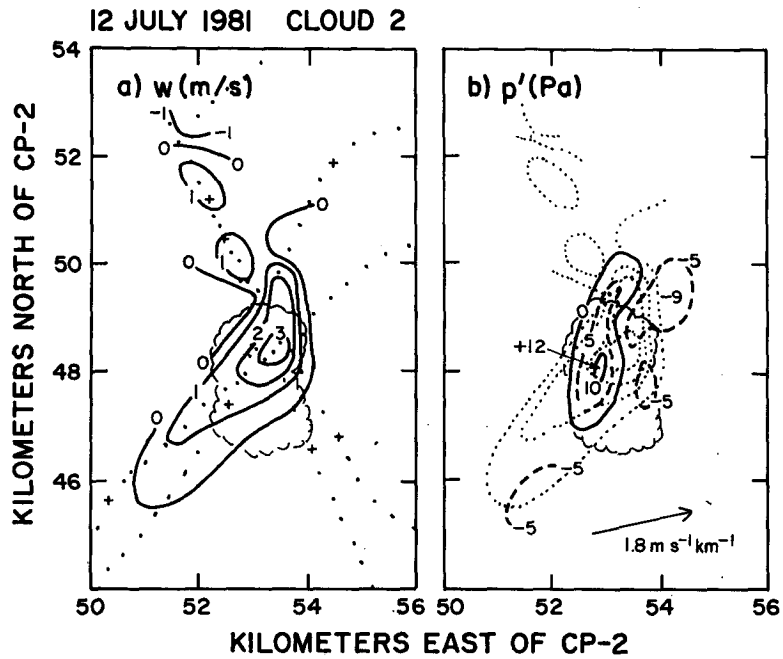

FIG. 5. As in Figure 4, but for cloud 2. Fields are in cloud-relative coordinates.

For the clouds in higher shear, we found that the terms involving the interaction of the updraft with the vertical shear of the horizontal wind, $2(\partial u/\partial z)(\partial w/\partial x) + 2(\partial v/\partial z)(\partial w/\partial y)$, dominated the pressure field. If this is so, and if the horizontal changes in the pressure field dominate, we can simplify (1) by assuming (i) $\partial u/\partial z = dU/dz$, and $\partial v/\partial z = dV/\partial z$, where U and V are the environmental wind and (ii) that $p \sim p_0 \cos[(2\pi/L)x]$, $w \sim w_0 \sin[(2\pi/L)x]$, where x is the direction of maximum pressure change, to obtain:

$$p_0 = \frac{w_0 L \rho_e}{\pi} \frac{dU_\nabla}{dz} \qquad (3)$$

where L is the horizontal wavelength of the vertical-velocity and pressure fluctuations, in the direction of the maximum pressure gradient, and dU_∇/dz is the vertical shear of the horizontal wind, also in the direction of maximum horizontal pressure change. The assumption (i) follows Rotunno and Klemp (1982), while (ii) follows from (i) and the observed quarter-wavelength lag between pressure and vertical velocity signals (LeMone et al. 1988).

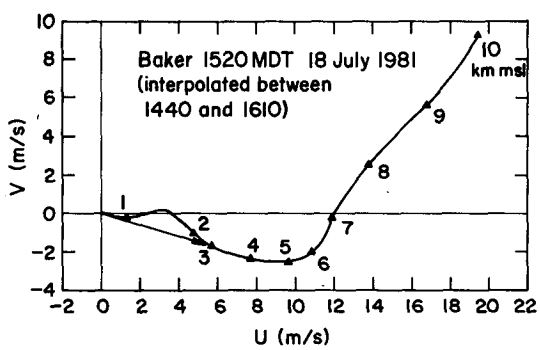

FIG. 6. Hodograph for 18 July cloud. Arrow indicates cloud motion. The cloud is less than 10 km from Baker. The wind at cloud base (2.8 km) equals cloud motion to within measurement accuracy.

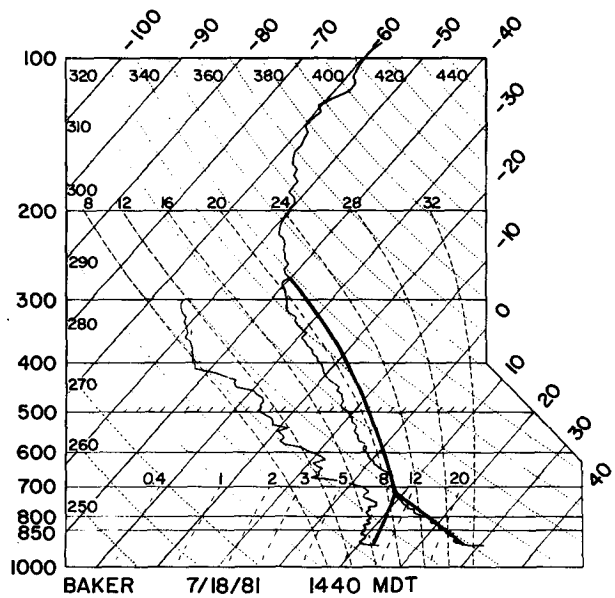

FIG. 7. Temperature and mixing ratio profiles and parcel trajectory corresponding to the hodograph in Fig. 6, plotted on a skew T–log$p$ diagram as in Fig. 3.

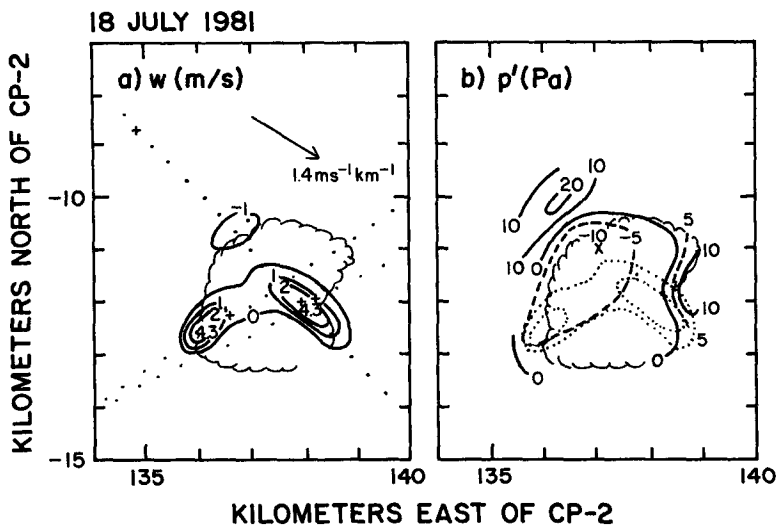

FIG. 8. For 18 July, just below base of cloud 2: (a) vertical velocity field, and (b) perturbation pressure field, with vertical velocity (dotted) superimposed. Cloud base is outlined in scallops. Fields are in cloud-relative coordinates. Vector indicates the vertical shear of the horizontal wind from Fig. 6, evaluated at cloud base. The two maximum values of w (4.3 m s^{-1}) are plotted.

The amplitudes of the pressure oscillation obtained from (3) for the three cases appear in Table 2. In the absence of an obvious shear-related pressure field, L and the shear dU_∇/dz for cloud 1 on 12 July are measured along the long axis of the flight pattern, since the pressure and vertical velocity gradients along this direction are the most certain. For the 18 July cloud, the shear is arbitrarily taken in the east–west direction. The updraft diameter L is largest in this direction, so that any effects from (3) should be maximized.

Clearly, the expected pressure oscillations from (3) are within the noise level. Note from Table 2 that the small updraft wavelengths and magnitudes, as well as the smallness of the shear, contribute to the small amplitude.

The small size and low speed of the cloud-base updrafts also reduces the *relative* importance of the terms representing the interaction between the updraft and the *mean* shear, since these terms are divided by the cloud-flow scale only once, while the updraft perturbation vertical shear terms

$$\frac{\partial u'}{\partial z}\frac{\partial w}{\partial x}+\frac{\partial v'}{\partial z}\frac{\partial w}{\partial y}, \quad u'=u-U, \quad v'=v-V$$

and the remaining dynamic terms in (2), involving primarily cloud-scale gradients, are divided by the square of the cloud-flow scale.

An a priori explanation for the suggested increase in the relative importance of buoyancy to the pressure field around the cloud-base updraft of these small clouds is not obvious. However, the apparent causes of their pressure fields are consistent with the place these clouds occupy in the spectrum of motions from the larger cloud updrafts of LeMone et al. (1988) to the smaller updrafts observed in the fair weather boundary layer. The clouds of LeMone et al. have updrafts with diameters ranging from 5 to 20 km across, with speeds varying from 5 to 10 m s^{-1}, while typical updrafts in the daytime boundary layer are less than 1 km across with maximum speeds of the order of 2 to 3 m s^{-1}. The three clouds discussed have updrafts 2 to 5 km across and vertical motions of 3 to 6 m s^{-1}. The cloud-base pressure perturbation around the updraft of the large clouds is of the order of 100 Pa and is largely due to the interaction of the updraft with the vertical shear of the horizontal wind. Numerical simulations of large eddies in the clear-air boundary layer show pressure perturbations of the order of 2 Pa for heat fluxes and boundary-layer depths typical of CCOPE.[1] (Deardorff 1974; Moeng and Wyngaard

TABLE 2. Calculation of perturbation pressure from (3).

Date	dU_∇/dz	L (km)	w_0 (m s^{-1})	ρ (kg m^{-3})	p_0 (Pa)
12 July–Cloud 1	1.7[a]	7[a]	2.5	.94	9
12 July–Cloud 2	1.8	4	2.5	.93	5
18 July	1.2[b]	<5[b]	2.5	.89	<4

[a] Along the cloud line, in the absence of an obvious updraft-shear-forced pressure pattern.
[b] East–west.

[1] 0.3 to 0.45°C m s^{-1} (Smolarkiewicz and Clark 1985), 1500 m (Table 1).

1986.) Applying CCOPE conditions to the nondimensional pressure field of the composite plume constructed by Wilczak and Businger (1984) from tower data, we find a maximum pressure perturbation of the order of 5 Pa. Both Moeng and Wyngaard (1986), and Wilczak and Businger (1984) find that buoyancy accounts for most of the pressure fluctuations. The pressure perturbations at the base of the three small clouds described here are of the order of 10 Pa and show the effects of buoyancy and shear–updraft interaction.

It is surprising that the three clouds analyzed here all have small diameters and shallow tops. These clouds were sampled because they were among the larger of their population, and a look at concurrent Skywater radar pictures reveals no larger echoes within 50 km. Yet the clouds are far smaller than would be expected from looking at the environmental soundings: the maximum potential cloud tops are above 9 km MSL for both days, as defined by the intersection of the parcel curve and the temperature sounding. The largest cloud, cloud 1 of 12 July, has a top at only 5.7 km and a base only 5 km across. Presumably, the smaller depths are the result of entrainment, which is inversely proportional to the updraft diameter.

We believe that the small horizontal dimensions, and thereby the small depths of the three clouds discussed, are related to the small vertical shear of the horizontal wind. Of the 40 clouds which had three or more aircraft legs flown under them in CCOPE, two of the three smallest occurred on 12 and 18 July. Examination of the remaining clouds supports the cloud size-shear relationship.

One possible mechanism for this relationship is cloud enlargement through the interaction of the clouds with cloud- and boundary-layer induced tropospheric gravity waves, as discussed by Clark et al. (1986), since this interaction becomes stronger with stronger cloud-base shear. We will deal with this relationship and several candidate mechanisms in a forthcoming paper.

5. Conclusions

The pressure fields around the cloud-base updrafts of three cumulus clouds in low-shear environments are compared to those for the higher-shear clouds studied by LeMone et al. (1988). The high-shear cloud-base fields were dominated by a high-low pressure couplet displaced 90° from the updraft, with the highest pressure upshear of the updraft and the lowest pressure downshear. The pressure extrema were typically around 100 Pa, with a range from 20 to 950 Pa.

In contrast, the cumulus clouds examined here have very weak pressure fields, with extrema of the order of 10 Pa. Only one cloud shows the effects of the updraft interacting with the shear, with high pressure upshear of the updraft and low pressure downshear. The pressure perturbation beneath the other two clouds appears to be influenced by the buoyancy of the air overhead, with the lowest pressure beneath the cloud. The small size and intensity of the cloud-base updraft is just as important as the shear in accounting for the weakness of the pressure field induced by shear–updraft interaction.

The apparent greater influence of buoyancy on these clouds reflects the position of their updrafts in the spectrum of motions from the updrafts of large thunderstorms to updrafts in the fair-weather boundary layer. In the former and in cumulus congestus, the interaction between the updraft and the vertical shear is important in determining the pressure field around the cloud-base updraft. In the smaller and weaker boundary-layer updrafts, buoyancy plays the major role in creating the pressure field. The updrafts feeding the three clouds described here are intermediate in size and intensity, and their pressure field shows the influence of buoyancy and shear–updraft interaction.

Acknowledgments. This research was made possible by the careful design and execution of flight patterns around growing cumulus in CCOPE, and the complete summary of these flights that was stimulated by James C. Fankhauser. We benefited from discussions with Drs. Jørgen Jensen, Richard Rotunno, and Edward Zipser, and the careful review of this manuscript by Dr. George Young. Garpee Barleszi made several suggestions that improved the figures. We wish to thank Frances Huth for typing and editing the manuscript.

REFERENCES

Clark, T. L., T. Hauf and J. P. Kuettner, 1986: Convectively forced internal gravity waves: results from two-dimensional numerical experiments. *Quart. J. Roy. Meteor. Soc.*, **112,** 899–925.

Fankhauser, J. C., G. M. Barnes, C. J. Biter, D. W. Breed and M. A. LeMone, 1983: Summary of NCAR Queen Air measurements beneath cumuli in CCOPE. NCAR/TN-207+STR. [Available from the National Center for Atmospheric Research, P.O. Box 3000, Boulder, Co. 80307.]

Madden, R., E. Zipser, E. Danielsen, D. Joseph, and R. Gall, 1971: Rawinsonde data obtained during the Line Islands Experiment. NCAR Tech Note TN/STR 55, 71 pp. [Available from NCAR, P.O. Box 3000, Boulder, Co. 80307.]

LeMone, M. A., and L. F. Tarleton, 1986: The use of inertial altitude in the determination of the convective-scale pressure field over land. *J. Atmos. Oceanic Technol.*, **3,** 650–661.

——, G. M. Barnes, J. C. Fankhauser and L. F. Tarleton, 1988: Perturbation pressure fields measured by aircraft around the cloud-base updraft of deep convective clouds. *Mon. Wea. Rev.*, **116,** 313–327.

Moeng, C.-H., and J. C. Wyngaard, 1986: An analysis of closures for pressure-scale covariances in the convective boundary layer. *J. Atmos. Sci.*, **21,** 2499–2513.

Rotunno, R., and J. B. Klemp, 1982: The influence of the shear-induced pressure gradient on thunderstorm motion. *Mon. Wea. Rev.*, **110,** 136–151.

Smolarkiewicz, P. K., and T. L. Clark, 1985: Numerical simulation of the evolution of a three-dimensional field of cumulus clouds. Part I: Model description, comparison with observations, and sensitivity studies. *J. Atmos. Sci.*, **42,** 502–522.

Wilczak, J. M., and J. A. Businger, 1984: Large-scale eddies in the unstably stratified atmospheric surface layer, Part II: Turbulent pressure fluctuations and the budgets of heat flux, stress, and turbulent kinetic energy. *J. Atmos. Sci.*, **41,** 3551–3567.